# We are IntechOpen,
# the world's leading publisher of
# Open Access books
# Built by scientists, for scientists

## 6,900
Open access books available

## 185,000
International authors and editors

## 200M
Downloads

## 154
Countries delivered to

Our authors are among the

## TOP 1%
most cited scientists

## 12.2%
Contributors from top 500 universities

**BOOK CITATION INDEX**
CLARIVATE ANALYTICS
INDEXED

**WEB OF SCIENCE™**

Selection of our books indexed in the Book Citation Index
in Web of Science™ Core Collection (BKCI)

## Interested in publishing with us?
## Contact book.department@intechopen.com

**Chapter**

# Full-Field Transmission X-ray Microspectroscopy (FF-XANES) Applied to Cultural Heritage Materials: The Case of Ancient Ceramics

*Philippe Sciau and Tian Wang*

## Abstract

Synchrotrons provide more and more significant analytical techniques to investigate ancient materials from cultural heritages. New ways to visualize the complex structure of these materials are developed on the basis of elemental, density, and refraction contrasts. The tunability of synchrotron beams owing to the high flux and high spectral resolution of photon sources is at the origin of the main chemical speciation capabilities of synchrotron-based techniques. Among them the full-field X-ray absorption near-edge structure (XANES) imaging technique using hard X-rays is particularly efficient. It allows investigating a significant volume of material with a very good spatial resolution, which is invaluable for ancient material because of their heterogeneity and complexity. After presenting the technique and its variants, we will show its ability to study cultural heritage materials through a few examples.

**Keywords:** FF-XANES, cultural heritage material, attic ceramic, Roman pottery, Chinese porcelain, Qinghua

## 1. Introduction

Recent decades have seen the tremendous increase in the use of synchrotron radiation-based techniques to study cultural heritage materials [1, 2]. The materials involved in ancient artifacts are very diverse including organic and inorganic compounds such as skins, textiles, woods, resins, stones, metals, alloys, glass, ceramics, or concretes to name only the most current. However, despite this great diversity, most materials used in the design of ancient objects have in common a significant complexity and heterogeneity compared to standard modern manufactured materials. This complexity is not only due to the chemical composition, which can involve a lot of elements, but especially comes from the spatial distribution and organization of these elements leading often to very complex structures. In fact, many of the materials developed by ancient civilizations can be assimilated to composite materials made of a large number of components presenting significant variations in composition, size, or shape. The spatial distribution of components is not so regular as in standard modern materials but it is not random. Often, the

components distribution shows a rather nice organization, which can even lead to partially hierarchized structure, which often plays a key role in the physical properties. In addition, the structuration of the components distribution at different scales from nanometer to millimeter is an invaluable source of information about the manufacturing process. This is a very important point since it is often the only main information source of manufacturing technology used for significant productions such as Chinese porcelain, Attic ceramic, *Terra Sigillata*, or Roman concrete to name a few. The equipment used to manufacture them was destroyed, and the structural remains discovered during excavations are often so degraded that it is very difficult to deduce some information concerning the facility operation. A few historical texts mentioning technical processes have been preserved until today. Unfortunately, these valuable documents are not always detailed or completed and moreover, often not written by manufacturers or users. To be really efficient, the study of these documents must be associated to physicochemical analyses of materials produced by the mentioned technologies. Actually, since the main remains left by ancient technologies are the produced materials, a reverse engineering-type investigation is the often best way to obtain pertinent data about manufacturing process [3].

A scientific discipline, called "archaeometry," is dedicated to the analysis of ancient artifacts by physicochemical ways. Many different techniques are used in routine, and for a few decades, a strong growth of nonevasive and portable techniques has been observed for analyzing materials of museum objects on site, without any damage. However, the analytical techniques requiring sampling or sample preparation continue to be developed, in particular the techniques allowing us to characterize the chemical composition and the structure at different scales such as the scanning and transmission electron microscopies (SEM and TEM) and of course the synchrotron radiation-based microscopies that we will present in detail in the next paragraphs. Materials constituting valuable artifacts can be found in many less precious pieces from which suitable tiny fragments can be sampled.

Synchrotron beamlines are, of course, nonportable facilities, but they can be used to directly analyze objects without preliminary sampling and without damage insofar as the analyzed area is not altered by the beam. However, if one wants to take full advantage of the latest developments in terms of high spatial resolution such as submicrometer to nanometer resolutions, it is often necessary to prepare samples with suitable sharps and sizes. These advanced technical platforms, specially beamlines combining X-ray imaging and spectromicroscopy such as ID21 at the European synchrotron radiation facility (ESRF) in Grenoble (France) for instance, are perfectly suitable for the detailed study of complex structure of ancient materials [2]. The large field of view (FOV) combined with a high resolution allows for characterizing the structural organization on large scale, typically from a few millimeters to a few hundred nanometers. Spatial resolution of a few dozen nanometers can be reached on some beamlines with a small decrease in the field of view. Up to now, nanometer resolutions are not yet available and require transmission electron microscopy. However, in many cases, the investigated scale range is large enough to provide a fairly detailed structural description allowing to deduce significant data concerning the manufacturing processes or the relationships between structure and physical properties [4]. The large-scale range also allows us to study some scale laws governing the structure, to identify the more pertinent scales according to a defined physical property and other parameters involved in the study of complex hierarchized materials. If the elemental composition can be studied at high resolution on the majority of micro- and nanobeamlines taking into account the beamline energy range of line and the targeted elements, it

is different for the mineral or crystalline phase composition. Structural composition can be determined from X-ray diffraction (XRD) or deduced from X-ray absorption spectroscopy (XAS). However, even if more and more beamlines propose the two techniques, they are seldom optimized for both. A choice must be done between the two approaches as much as the diffraction requires associating monochromatic (powder) and polychromatic (single crystal) diffractions to be efficient. In XRD experiments, the spatial resolution is given by the size of the X-ray beam. With a beam size of a few microns or smaller, only the crystallites with sizes very inferior to the beam size give a usable diffraction pattern in monochromatic mode; X-ray powder diffraction conditions. The study of larger crystals relative to the beam size requires polychromatic beam in order to record a large number of reflection on the 2D diffraction pattern to be able to identify the nature and the orientation of the crystallite (or a few crystallites) irradiated by the beam; X-ray Laue diffraction conditions. This coupled diffraction approach applied to the cultural heritage materials is detailed in [5]. In this chapter, we will present only the approaches based on X-ray absorption spectroscopy, which currently give the best spatial resolutions and are much less time-consuming.

## 2. X-ray full-field XANES analysis

Usually, the high spatial resolution is obtained by focusing the X-ray beam on the sample surface as much as possible in order to have the smallest probed area, for instance, the smallest irradiated area, on ID21 (ESRF), down to a rectangle of around 300 nm (V) × 700 nm (H), using a focusing Kirkpatrick-Baez mirror system. The irradiated area can be decreased for monochromatic X-rays using zone plates ("ZP") at the expense of flux, chromaticity, and beam stability [2]. Detectors positioned around the sample allow for recording transmitted beam intensity and the X-ray fluorescence (XRF) emission. μXRF 2D-mappings are obtained by raster-scanning the sample over areas of interest and recording the signals with different detectors. Element maps are quickly obtained from the XRF emission. Punctual X-ray absorption spectra (XAS) can be easily obtained directly from the measurement of the intensity of the transmitted beam versus the energy of the X-ray incident beam, if the sample is thin enough, or deduced from the evolution of the intensity of XRF emission versus the energy of incident beam. Depending on the characteristics of beamlines, the available energy range around an atom absorption edge can be limited to the near-edge energy range and thus only the X-ray absorption near-edge structure (XANES) spectrum is accessible or on the contrary, large enough to allow the full recording of extended X-ray absorption fine structure (EXAFS) spectrum. In theory, nothing prevents to acquire step by step all the XANES spectra of a 2D mapping with the exception of the recording time. One square millimeter mapping with a pixel of one square micrometer requires the recording of one million spectra. The acquisition of one spectrum requiring a few minutes with standard detection systems and several days would be necessary to record such a map. Except with ultrafast detectors [6], the reconstruction of pixel XANES spectra from the scanning of area at the different energy is not faster. Actually, in addition to the element maps, only the valence state maps of elements can be obtained since it requires scanning the sample area only for a few number of energy around one absorption edge of the selected element. The recording of full XANES spectra is uniquely reserved for a few points of the map. To obtain the XANES spectra of a square millimeter area with a submicrometer resolution, that is, a few millions of XANES spectra with reasonable acquisition times, an approach of full-field type has been developed that we are now going to describe.

## 2.1 Full-field XANES (FF-XANES) analysis with nonfocused beam

Instead of scanning the interest area with a focused micro (or submicro)-X-ray beam, the interest area is directly illuminated using a larger beam, which can be obtained in removing all focusing optics as this is performed on ID21 (lensless setup) [2]. On this beamline, the sample X-ray radiography is recorded with a detection system consisted of a scintillator and a CMOS camera coupled to a long working distance optical objective in order to record a magnified transmission image of the sample. Two objectives with different magnification (10× or 20×) can be used, leading to a pixel size of $0.65 \times 0.65 \ \mu m^2$ or $0.32 \times 0.32 \ \mu m^2$ and a field of view of $1.5 \times 1.5 \ mm^2$ or $0.75 \times 0.75 \ mm^2$, respectively, for the 10× and 20× magnifications.

The 2D-XANES map of a selected element is obtained by recording a series of a few hundred X-ray radiographies at different energies, the energy being tuned in small steps (0.2–10 eV) across the absorption edge of selected element. Then a data preprocessing, including image alignment, normalization, and several other corrections, allows for creating the full-field XANES data set, which represents a 3D radiography stack consisting of a few hundred images recorded at different energies. Therefore, each pixel contains a full high-resolution XANES spectrum [2, 7].

## 2.2 Full-field XANES in transmission X-ray microscopy

The advent of high-performance X-ray sources and the improvement in the X-ray lens objectives allowed the development of transmission X-ray microscopy (TXM) using hard X-rays with spatial resolutions down to 30–40 nm and 15–30 μm FOV [7–9]. As previously, this type of device can be used to record a series of radiographs through the absorption edge of an element of interest. Besides the difference of spatial resolution and FOV, the data preprocessing is little more different because of the more complex design involving several X-ray lens whose focal lengths are energy dependent. In fact, the data processing is nontrivial and it is only with the design of new algorithms at the beginning of this decade that it was possible to obtain usable chemical images from TXM [7]. Currently, these algorithms are well integrated in most preprocessing software available on the TXM beamlines, or in data processing software such as TXM-Wizard package. Like the pixel size and the FOV are energy dependent, the spatial resolution and the FOV of 2D XANES image are, however, limited to the smallest FOV and the largest pixel size of image series. The concept of XANES microcopy is illustrated in **Figure 1** of Ref. [7].

Most of the software allow us to combine several image series in order to obtain a larger 2D XANES image and thus to investigate an area larger than the FOV of TXM used. However, this mode (called mosaic mode) can be rapidly time consuming and for investigating large areas, it can be more efficient to scarify the resolution and to use the nonfocused geometry outlined in the previous paragraph (Section 2.1).

## 2.3 Data processing

A 2D XANES image contains several millions of XANES spectra, and it was necessary to develop specific collections of programs to process these huge data, which were integrated in existing software package as, for instance, in PyMca package [10] or gather in new software such as in TXM-Wizard [11]. The latter was used for data processing of examples described in the next paragraphs. The reference described in detail the main features of toolkits available within the package. This software can be downloaded free from its web page https://sourceforge.net/projects/txm-wizard/ as well as reference papers.
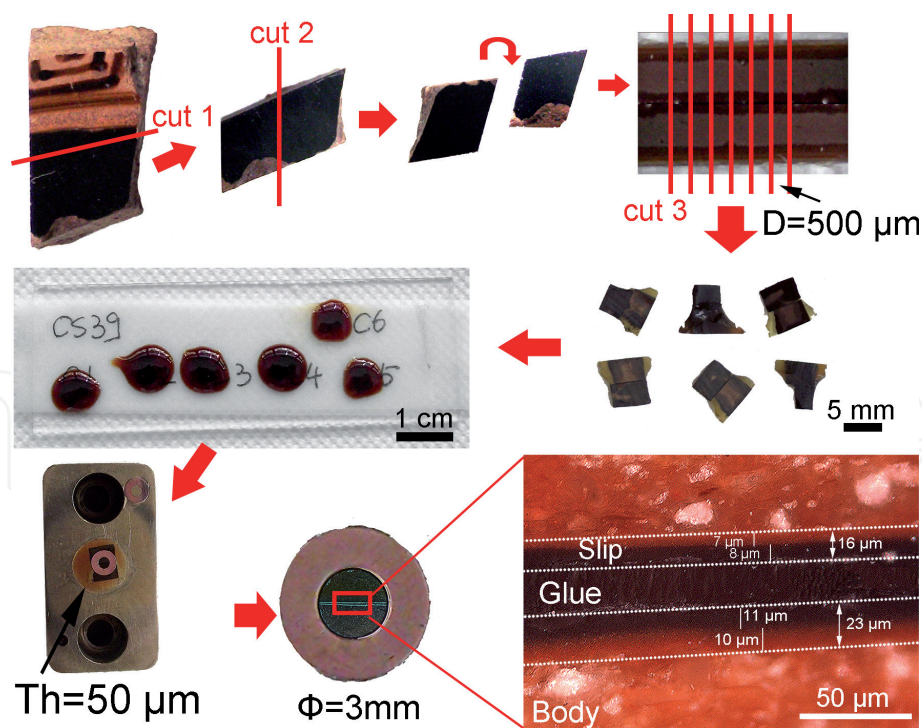
**Figure 1.**
*Main steps in the cross-section sample preparation process for full-field XANES analysis. From left to right: (1–2) cutting using a wire saw in order to obtain (3) two strips with black decors, (4) sandwich making using glue, (5) cutting thin lamella (500 μm), (6) protection with glue, (7) mechanical polishing down to 40–50 μm, (8) adding a reinforcing Cu washer, and (9) finally optical micrograph of central area.*

## 3. Cultural heritage materials studies: some examples in ancient ceramic field

To illustrate the power of FF-XANES analysis in the cultural heritage field, we chose to focus our purpose on ceramic material, one of the first synthetic materials made by human communities. Ceramic artifacts are also one of the most studied objects by the archeologist community [3]. Often produced in large amount by quite controlled manufacturing processes, this material is perfectly well suitable for in-depth studies inquiring sampling and specific sample preparations. Mass production gives easily access to material, and the control of manufacturing processes allows for limited investigations to a small corpus.

### 3.1 Iron speciation in Greek and Roman potteries

The first example concerns the Attic and Campanian potteries produced during the Greek and Roman periods, respectively. These two types of tableware are characterized of a red body partially or totally covered with a thin black high-gloss coating. Red body and black coating were obtained both from two different Fe-rich clay preparations and fired together using a complex firing protocol (lost now) allowing to obtain $Fe^{2+}$-based crystals in coating and $Fe^{3+}$-based crystals in body. Since the late eighteenth century, diverse protocols have been proposed, and even if the firing protocol in three steps (oxidative°➡°reductive°➡°oxidative) theorized by Noble in 1965 is commonly accepted, the understanding of this technology is still too limited, especially to follow evolutions or adaptation to the local raw clays. As many fragments of these ceramics have survived to the present day, the use of investigation techniques requiring the preparation of suitable samples is not a problem but a good way to recover information on this lost technology [12].

### 3.1.1 Sample preparation

The FF-XANES analysis being performed in transmission mode, the best sample shape is a thin parallel-faced lamella. The lamella orientation depends on the sought information and its thickness can be estimated taking into account the concentration of the selected element and the average elemental composition. The global composition allows for calculating the X-ray transmission before the absorption edge, while the concentration of the selected element allows us to estimate the absorption edge height, in the same way as commonly performed for XANES measurements in transmission mode.

In the presented examples that have been partially published in Refs. [13, 14], the element of interest was the iron and the K-edge was chosen. The orientation of blade was chosen for studying Fe speciation from the sample surface to the body. The average composition of the coatings leads to a calculated optimal thickness of about 20–30 μm, while the one of the body (lower Fe rate) is around 40–50 μm. The intensity of incident X-ray beam being higher at the center, the surface coating has been placed at the center of the blade using a preparation method derived from transmission electron microscopy. The main steps of sample preparation are shown in **Figure 1**.

### 3.1.2 FF-XANES analysis

The radiographies were recorded on ID21 at ESRF using the 20× objectives, and the data preprocessing allowing to create the FF-XANES stacks was performed with the in-house software package PyMca [10] using the image realignment described in Ref. [15] and now included in the PyMca package. The closer data analysis was carried out using the TXM-Wizard software following the process described in Ref. [11]. **Figure 2(a)** shows one of the radiographies recorded before the Fe K-edge (at 7070 eV). The glassy coating appears as a dense and homogeneous layer of around a few tens microns, while the body reveals a more heterogeneous and porous structure. The first information, which can be extracted without further data processing, are the edge height and the edge energy position of all pixels (**Figure 2**). Filters allow for removing pixels for which either the edge height is too small regarding the noise level or the spectrum cannot be normalized. These pixels, as the pixels of glue, correspond to the iron-free areas or in too weak Fe concentration areas to give a XANES spectrum. The edge height map, correlated to the iron concentration, shows pretty well the difference in concentration between the coating and the body. It gives the same information as an element map of Fe. The edge energy position is proportional to the valence state: low energy corresponds to $Fe^{2+}$ and higher energy corresponds to $Fe^{3+}$. The difference between the coating and the body is obvious and in accordance with their respective color.
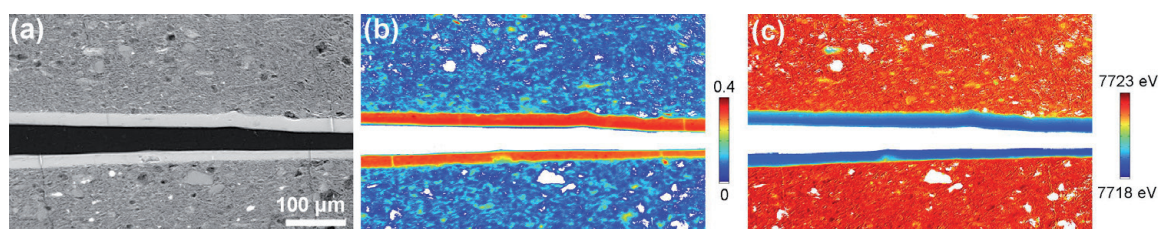


**Figure 2.**
*First steps of data processing: (a) radiography image recorded at 7070 eV, that is, below the Fe-K absorption edge. The images were collected at ESRF beamline ID21 in transmission mode with a total FOV of 332.16 × 522.24 μm² (1038 × 1632 pixels). (b) Edge jump map linked to the Fe rate and (c) edge energy map linked to the iron state valence calculated from the XANES spectra evolution. The scale bar for (b) reports the values of the (absorption) edge jump, defined as the difference between the average intensity value in the XANES postedge region and the average intensity value in the XANES pre-edge region. The scale bar for the maps shown in (c) indicates the energy of the (absorption) edge in eV.*

The study of the iron speciation needs a further analysis since it requires the use of the whole XANES spectrum and not only two parameters (height and energy position of jump edge) deduced from this spectrum. The number of pixel spectra is too huge (close to 2 millions) to consider an individual treatment. TXM-Wizard software proposes two approaches for a closer inspection of the set of XANES spectra: (i) a principle component analysis (PCA) followed by a *k*-means clustering or (ii) a least squares linear combination (LSLC) fitting with standards associated to a R-factors correlation analysis [11]. The first approach allows us to obtain a first result with open-minded solution. Here the PCA results show that the first four components (**Figure 3**) allow a rather good system description. Indeed, the first two components represent already a percentage of 99.6 and with the two others the value is about 99.8%. The *k*-means clustering, with k = 4, leads actually two different types of XANES spectra (**Figure 4a**). A clustering, with k > 4, does not give more different cluster types. The first cluster includes all the XANES spectra related to the coating, while the other clusters correspond to the body (**Figure 4b**). The XANES spectrum associated to cluster one shows some characteristics of hercynite ($FeAl_2O_4$) and magnetite ($Fe_3O_4$) reference spectra, while the three others are very close to maghemite ($\gamma$-$Fe_2O_3$) spectrum. The fitting of cluster 1 spectrum leads to 23% hercynite and 77% magnetite. The fitting of the two other cluster classes leads to similar results with 94–96% maghemite, 3–2% magnetite, and 3–2% hercynite. Even if hematite ($\alpha$-$Fe_2O_3$) was not found in the clustering approach, this phase was considered in the LSLC fitting with standards for being sure that it is not present in some small areas, which was confirmed by the detection of no measurable amount of hematite (**Figure 5**). Maghemite is the main iron-based phase of body with a rate almost everywhere above 90%. In the coating, hercynite and magnetite share the Fe ions in an H/M ratio varying from 1 to 2. A few differences can be observed between
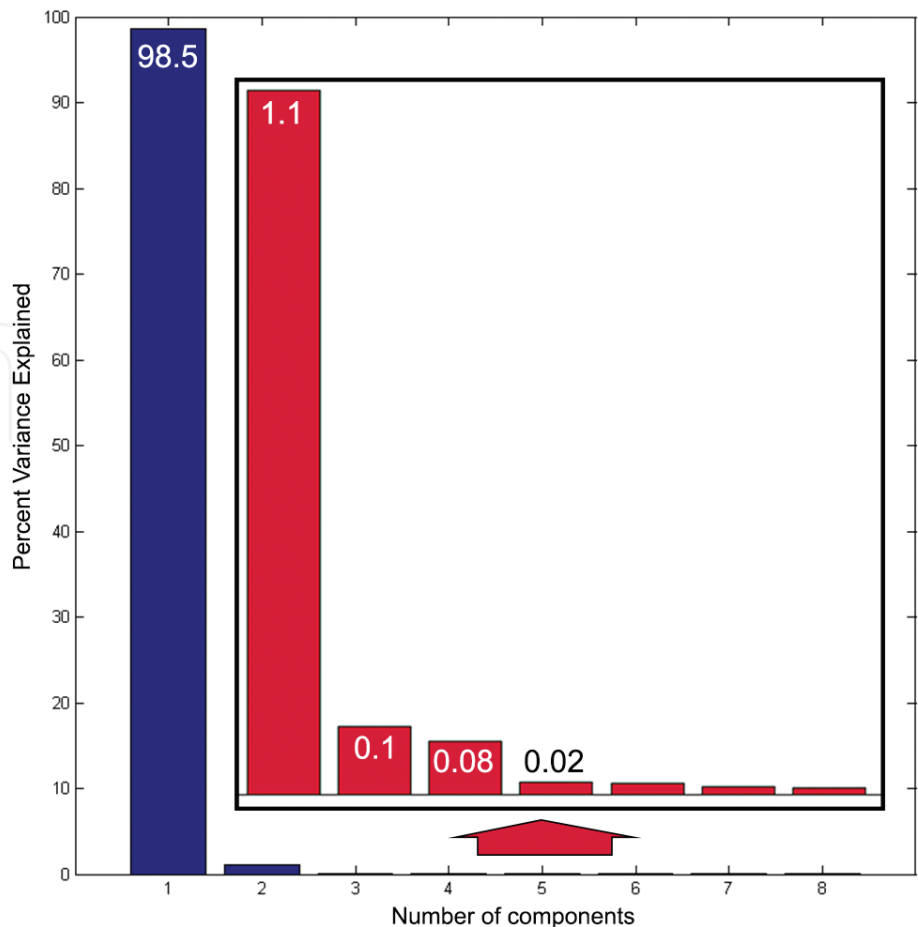


**Figure 3.**
*Result of PCA analysis showing the contribution of the first principal components highlighted in blue color.*
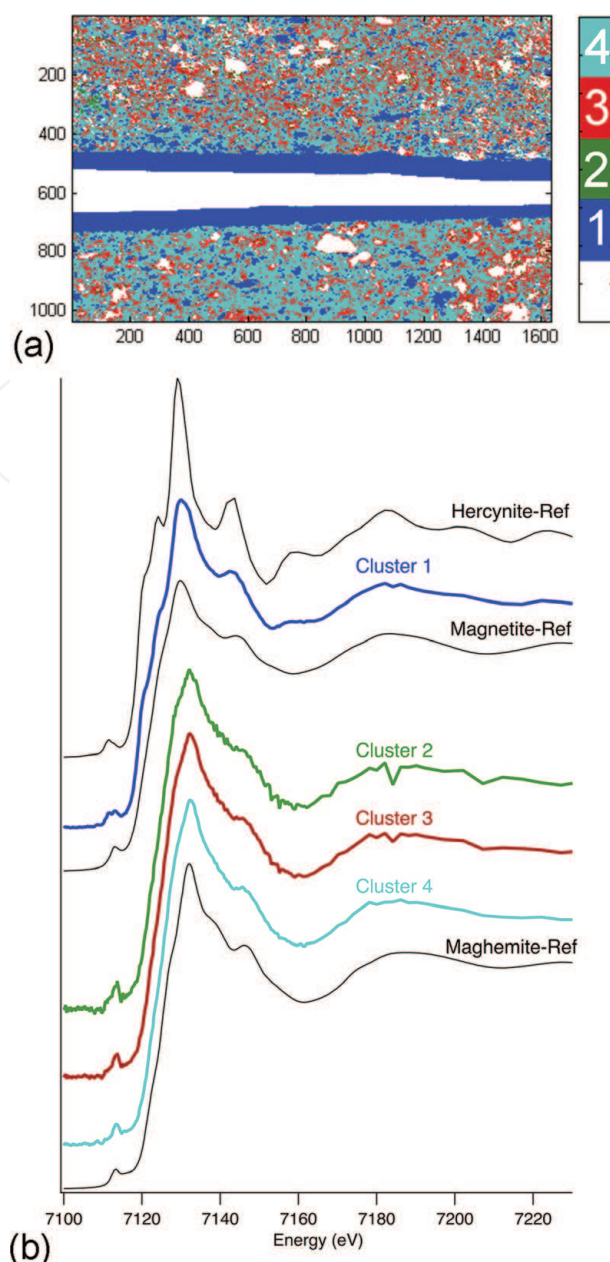
**Figure 4.**
*(a) Result of clustering and (b) the associated spectra compared to spectrum references. The references of hercynite, magnetite, and maghemite are taken from ALS database.*

the external (top) and internal (bottom) coatings. In the two cases, the hercynite concentration is higher in the upper part of coating (close to the surface), but the external coating exhibits a clear reoxidation of its surface, which is marked by the presence of a thin maghemite layer at its surface. The trichromatic phase map, excluding hematite, is shown in **Figure 6a** and compared to the map obtained for a Campanian ceramic fragment of Roman period. The detailed analysis for this last case can be found in Ref. [13].

The coating of Campanian contains mostly hercynite with only a few amount of maghemite mainly located at some surface areas, while the coating of Attic contains both hercynite and magnetite. In both cases, maghemite is the main Fe-based phase of the body but it is associated with a significant amount of hematite or hercynite in localized areas of Campanian body. These differences do not come from small variations in chemical composition between these two types of potteries, made at different places and times from similar but, however, different raw materials. They are actually due to the firing conditions. The iron valence repartition, mostly $Fe^{2+}$ and $Fe^{3+}$ in the coating and body, respectively, is consistent with the Noble's
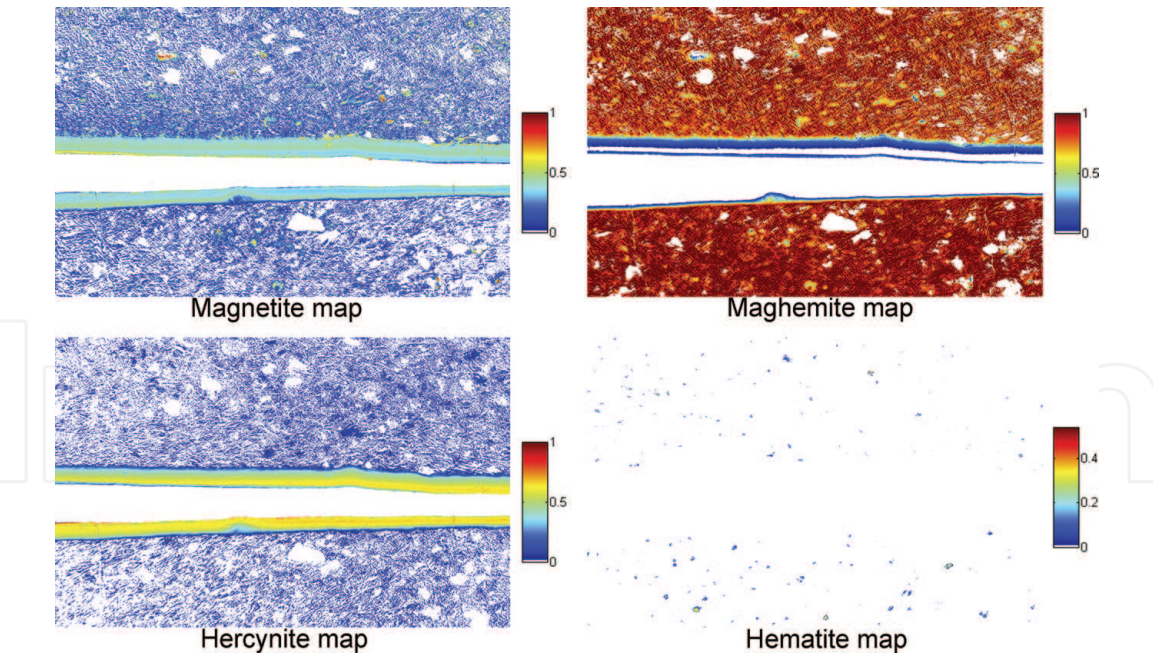
**Figure 5.**
*Phase maps obtained from the least squares linear combination fit of reference XANES spectra for magnetite, maghemite, hercynite, and hematite for each single pixel.*

protocol. During the reducing step (step 2), the highest temperature of the firing is achieved and a significant part of iron is $Fe^{2+}$; $Fe^{2+}/Fe^{3+}$ ratio increases with the temperature. The coating has a lower glazing temperature than the body and thus is also glazed during this step. Consequently, much more limited chemical reactions occur between the coating and the kiln atmosphere compared to the body and the kiln atmosphere during the last oxidative step achieved at a lower temperature than in the step 2. Then, during this last step, the body is mainly oxidized and turns red. The higher rate of hercynite and the absence of magnetite in the glazed coating of Campanian indicate that the temperature during the step 2 was higher here than for Attic. On the other hand, the presence of maghemite in some areas of the coating indicates that the chemical reaction between the coating and the kiln atmosphere was stronger during the last step. Maghemite is not distributed in a thin surface layer as in the exterior Attic coating but it is distributed in depth in some localized areas. The amount in these areas is also higher. This feature seems to be due to worse glazing of the Campanian coating. Coatings are made from the fine part of raw clay, and the selected part for the elaboration of Attic coating was
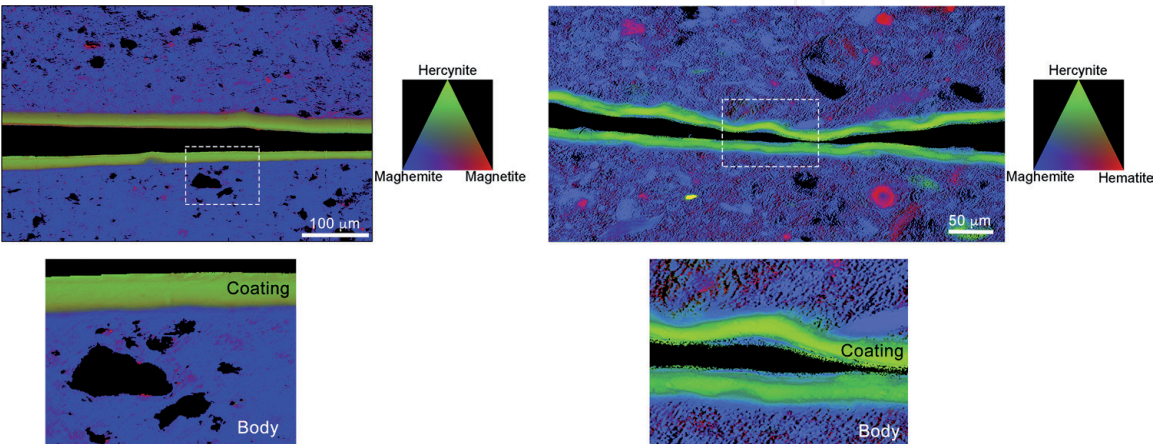


**Figure 6.**
*Comparisons of the phase maps of Attic (left) and Campanian (right) ceramics [13, 14].*

9

finer than for Campanian as revealed by quartz crystals sizes. Also, even if the two coatings have close elemental compositions, the glazing temperature of Attic coating is lower. The use of less fine part with larger grains of sand (mainly quartz) increases the porosity of glazing coating and then enhances its oxidation rate under the oxidizing atmosphere of kiln. The presence of hematite in the Campanian body is consistent with an oxidation at higher temperature allowing a partial transformation (or recrystallization) of maghemite into hematite. The hercynite-rich zones of Campanian body correspond to partially glazed zones, which did not be therefore completely reoxidized during the last step.

A thin blade prepared from the same Campanian fragment was also analyzed using the transmission X-ray microscope of 6-2c beamline at the Stanford Synchrotron Radiation Lightsource (SSRL), SLAC National Accelerator Laboratory [13]. The differences are only related to the characteristic differences between the two beamlines, that is, a smaller FOV and a better spatial resolution (about one order of magnitude) at Stanford. The FOV can be enlarged using the mosaic mode, which consists of recorded several series of radiographies with overlapping areas in order to obtain a 2D XANES map larger than the FOV. However, the investigated area cannot reach the FOV of ID21. In the problematic presented here, the better resolution does not bring much more in the iron speciation study and the larger FOV of ID21 shows a best advantage. On the other hand, the very good resolution of 6-2c beamline allowed for studying the sample porosity and for showing that hercynite was distributed in well-glazed dense zones. Maghemite is present in zones of greater porosity confirming that the hercynite is formed during the step 2 before the glazing. The maghemite comes from the oxidation of the last one, which is in contact with oxygen thanking to the open porosity during the step 3. A study of a presigillata fragment was also carried out at SSRL [13]. This type of pottery, which was also made during the Roman period but a century later than the Campanian productions, presents also a glazed black coating covering a red body. The results revealed both a high concentration of hercynite in the coating and a significant rate of hematite in the body. The top layers of the coating showed also a strong reoxidation with a significant presence of maghemite at the surface. The firing temperature during the step 2 was similar to the one of the analyzed Campanian but the oxidizing step 3 seems to start at higher temperature.

To conclude with this explanation of the problematic, a few words will be given on a recent study, which suggests that more complex firing protocols would have been used for some Attic productions [16]. The study was carried out on microsamplings coming from a decorated fragment attributed to the Berlin's painter and belonging to the collection of the J. Paul Getty Museum showing as well the actual possibility to use this technique to study precious samples. The analyzed fragment presents in some areas a red coating under the black coating ([16], **Figure 1**). FF-XANES investigation revealed that this red intermediate coating contained mainly hematite, while hercynite and maghemite were found in the black coating and the body, respectively ([16], **Figure 2**). The massive presence of hematite in this intermediate coating, whose chemical composition and the porosity are identical to the ones of black coating, was not considered as consistent with the firing protocol proposed by Noble. This firing protocol would have led to the same mineral composition for the two coatings. Also the authors proposed a more complex protocol involving two separate firings.

### 3.2 Under glaze decors of Chinese porcelain

In the first example, the average elemental composition and the concentration of the selected element, in this case iron, were quite suitable to transmission mode

measurements. This technical analysis can be also successfully used to study the speciation of an element in low concentration with, however, some restrictions as described in this second example. This example concerns the speciation of the coloring elements of the famous blue and white porcelain produced during the Ming Dynasty (1368–1644 AD).

Blue and withe porcelain (**Figure 7**), so-called Qinghua porcelain, is characterized of a brilliant white translucent glaze with a blue pattern painted underneath. The color is due to cobalt, but other transition metal elements including iron and manganese are also present in the Ming productions [17] and the aim of study was for establishing the feature of each [18].

*3.2.1 Sample preparation*

The thin parallel-faced blades were made as previously described (cf. Section 3.1.1) expect that it was not possible to determine an optimal thickness from the average element composition. The average concentration in transition elements (Fe, Mn, and Co) is very low (≤1%) and necessitates a thick sample superior to 500 µm to have a right edge jump at the K-edge of cobalt, for instance. Unfortunately with such a thickness, the absorption of these other elements (Al, Si, K, and Ca) limits the transmission in the energy range to a few percent and does not allow measurements in transmission mode. Also to conserve a right transmission in the investigated energy range, the sample thickness was chosen between 40 and 60 µm [18]. A sample ready for investigation is shown in **Figure 8**.



**Figure 7.**
*Qinghua porcelain, Mieping vase with "Eight dragons among the clouds." Ming Dynasty (1368–1644), Yongle reign (1403–1424), Jingdezhen workshop (Jiangxi province, China). Provenance: Estate of Jutta Frieda Luise Meischner and Bolurfrushan Family, Inv.-Nr. MBS 06/16–6.9.02 (© Æli Barjesteh, ASET Stiftung).*
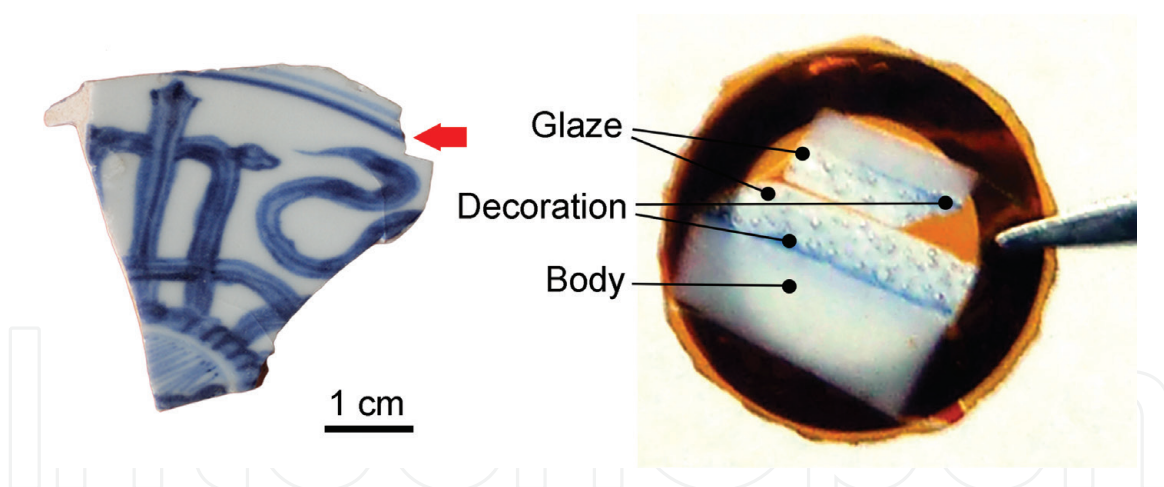
**Figure 8.**
*Sample for FF-XANES analysis (right) obtained from a fragment of Ming blue and white porcelain (left). For the preparation method, refer to* **Figure 1**.

### 3.2.2 Investigations

X-ray absorption spectra (XAS) collected in fluorescence mode are better suited for determining the speciation of elements in low concentration [19]. Unfortunately, the scanning of a large zone with a submicrometric resolution is too time-consuming for analyzing even a few samples. Also the technical advantages of the two techniques were combined.

At first, XRF maps were collected in scanning mode on large areas. The PyMca software was used to batch-fit the XRF spectra, to generate the elemental maps (from Na to Co) and to normalize these maps taking into account the incident beam intensity [10]. A typical result showing the main differences of elemental distribution in the various layers of a Ming Qinghua porcelain is presented in **Figure 9**. The colored zone is clearly identified by the high rate of calcium. The localized high concentrations in silicon correspond to quartz grains, which are more numerous in the body than in the glaze. The needle-shape crystals observed in the colored zone containing calcium are anorthite crystals [20]. The distribution of three transition elements (Mn, Fe, Co) is quite different. Mn and Co distributions are concentrated in colored areas confirming there are well contained into the pigment. However, Mn distribution is more uniform and does not present local high level compared to Co element. Fe is quite homogeneously distributed both in colored area and in above glaze. Laboratory XRF measurements revealed that the glaze areas without blue decors contain similar Fe rates [18]. A few punctual XANES spectra were acquired at the Co K-edge both over Co-rich particles and diluted Co in glassy matrix, by scanning the energy of the incoming beam and measuring the X-ray fluorescence signal of Co K-lines. For Co-rich particles, the recorded spectra were similar to the one of cobalt aluminate crystals ($CoAl_2O_4$), while in lower concentrated zones, the recorded spectra correspond to $Co^{2+}$ diluted in glass ([18], **Figure 5**). These spectra were acquired only for a few points. In order to have a full 2D picture of Co speciation and in particular to verify that all Co-rich particles are cobalt aluminate and not cobalt oxide phase, FF-XANES maps were acquired in a second step.

Series of radiographies were recorded through the Co K-edge, and the data processing was carried out as previously described. **Figure 10** shows one of the obtained results. The edge energy position map confirmed the presence of the only one state of valence and the phase map, the two types of cobalt speciation, that is, $Co^{2+}$ in the glassy matrix and $Co^{2+}$ in cobalt aluminate crystals. This last map was obtained by LSLC fitting after a PCA analysis and $k$-means clustering revealing the existence of only two types of XANES spectra. However, for the majority of the
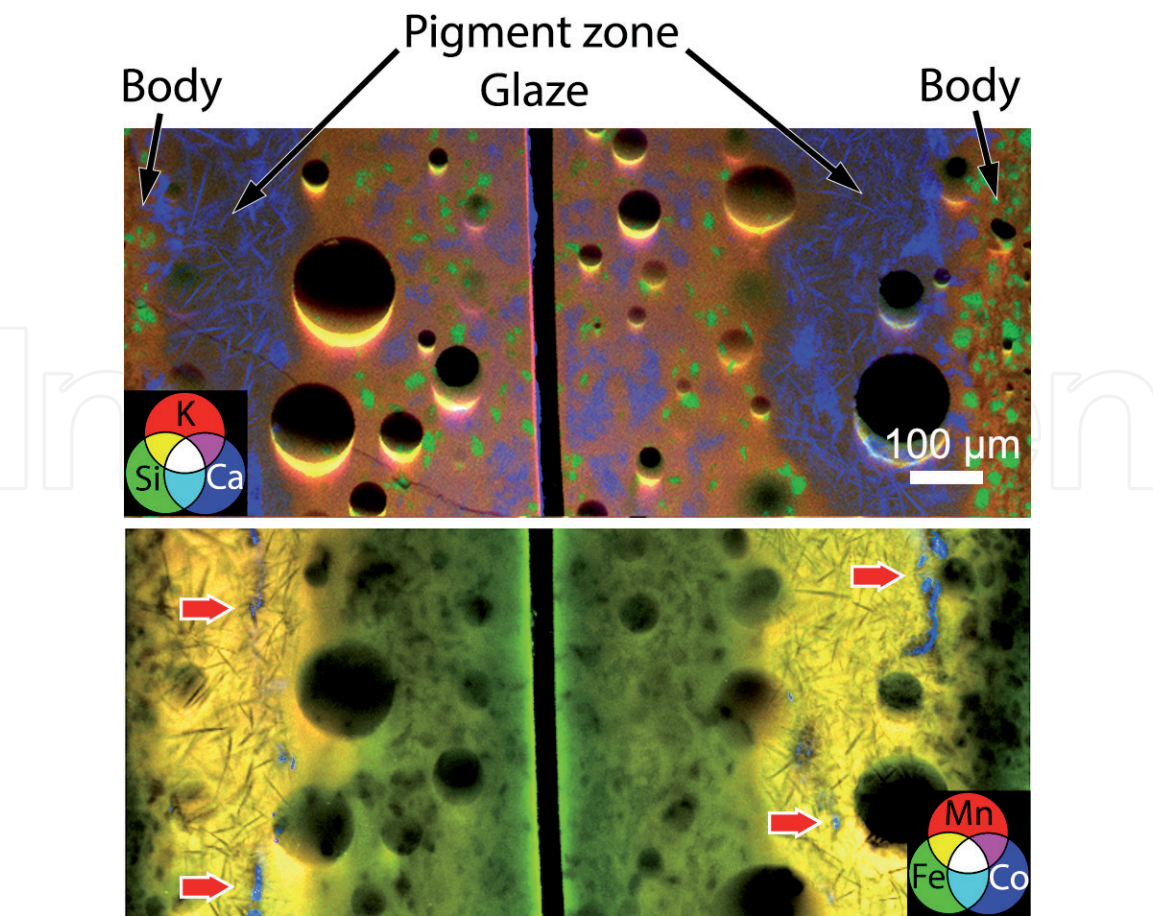
**Figure 9.**
*Tricolor elemental maps obtained from μSR-XRF measurements performed on ID21 beamline at ESRF [18].*

investigated zones, only Co-rich particles were studied. The cobalt concentration outside the particles was too low to give worktable pixel XANES spectra. For two samples, the Fe level was high enough to allow FF-XANES investigations at the Fe K-edge. The results confirmed the absence of Fe-based particles and a rather homogeneous distribution around the long narrow strips (anorthite crystals) and the cobalt aluminate particles. No variance of the edge energy was observed and the PCA confirmed the existence of only one type of XANES spectrum close to the one of bivalent iron dispersed in a glassy matrix [18]. Micro-X-ray diffraction is also available on ID21 beamline and was used to identify the phase structure of crystals. These measurements have also revealed that Co is partially substituted by another metal element in cobalt aluminate crystals.

To conclude this first part, X-ray scanning microscopy associated to FF-XANES analysis is an efficient way to determine the complex structure of underglaze decors



**Figure 10.**
*FF-XANES investigation performed on ID21 beamline at ESRF [18]. (a) Transmission image recorded at 7670 eV, (b) edge energy map, (c) phase map obtained from the least squares linear combination fitting (standards $CoAl_2O_4$ and Co in glaze) of each single pixel.*
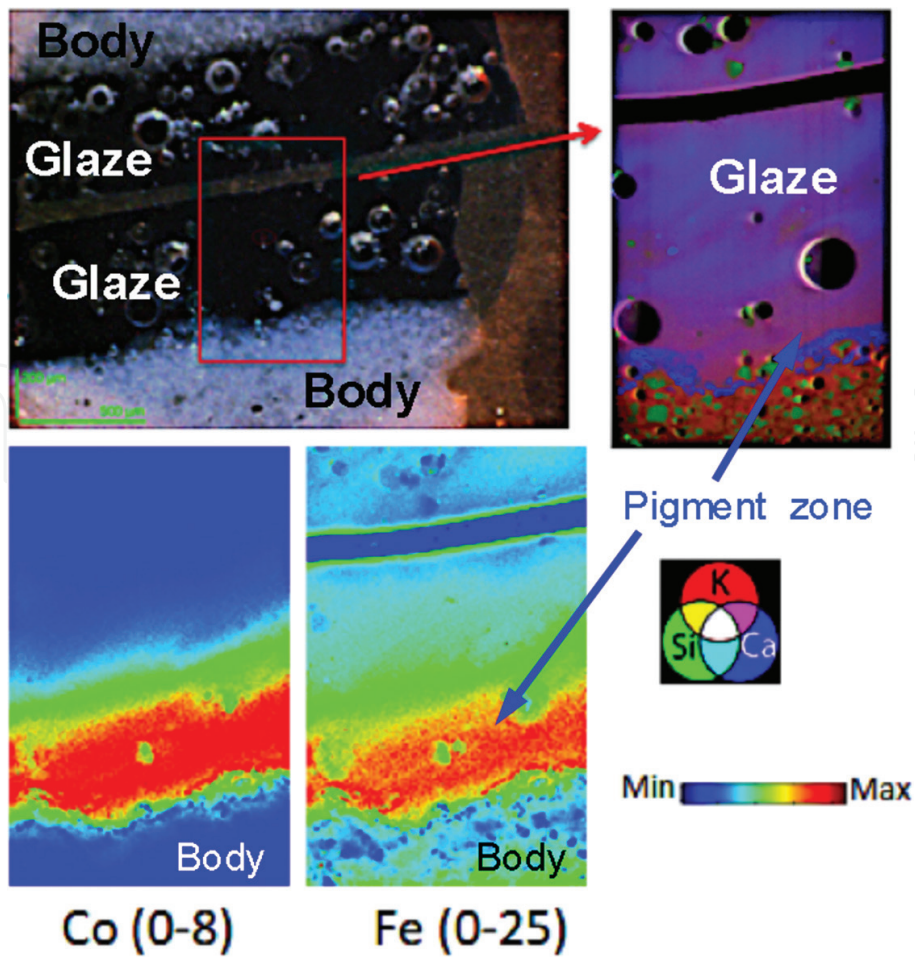
**Figure 11.**
*Typical elemental maps of a Yuan sample obtained from μSR-XRF measurements performed on ID21 beamline at ESRF. The transition elements (Co, Fe) are concentrated inside the pigment zone.*
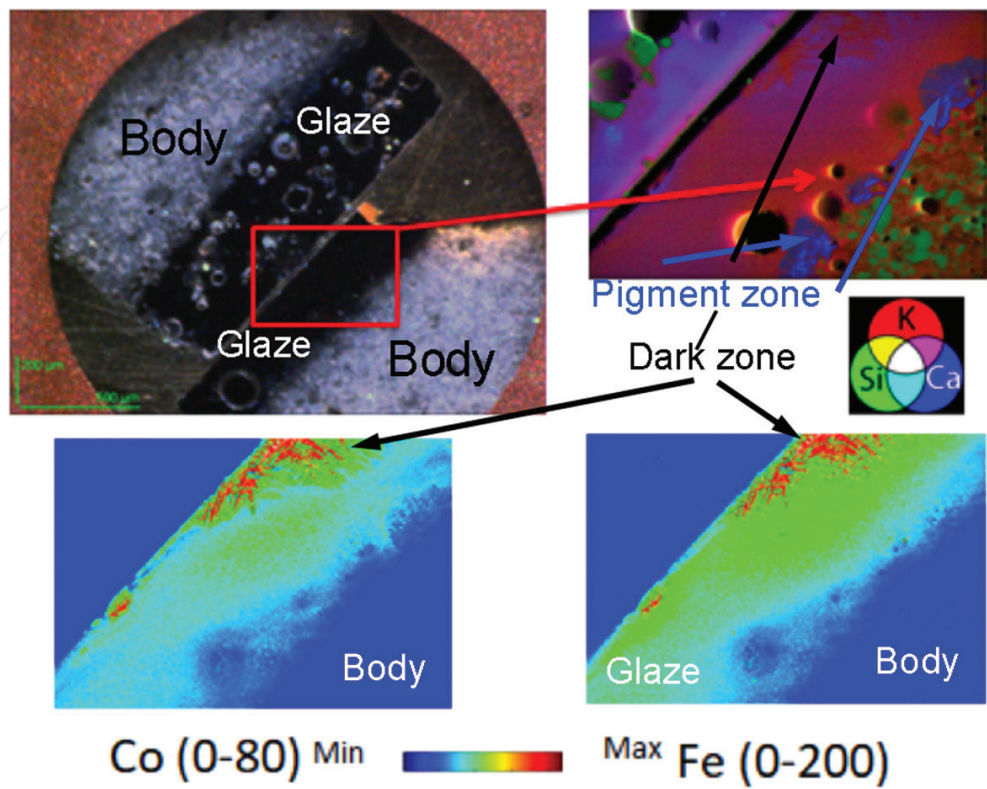


**Figure 12.**
*Elemental maps obtained from a dark zone showing the $CoFe_2O_4$ dendritic crystals.*

of Chinese ceramics. It allows not only to identify the color pigments and the speciation of colorant ions but also to observe how they are distributed in the glaze matrix.

These interesting first results led us to analyze previous productions made during the Yuan Dynasty (1269–1378 AD), which is considered by historians as the heyday of this type of porcelain. The elemental compositions of the two types of productions are quite close, except for Yuan blue color, which contains no Mn and much more Fe as confirmed by the elemental maps deduced from the X-ray fluorescence emission collected in scanning mode. The spatial distributions of the main elements (Al, Si, K, and Ca) are similar to the ones of Ming samples. The main difference concerns only the distributions of transition elements (Fe and Co). A higher concentration of Co clearly appears in the colored area close to the body/glaze interface, but the distribution is quite homogeneous unlike for Ming samples (**Figure 11**). No Co-rich particle was found in this area. The Co distribution is only diffuse and similar to the one of Fe element. In some cases, high punctual Co contents were only observed at the top surface and always associated to high Fe content as shown in **Figure 12**. In fact, these specific zones correspond to the dark spots visible at the surface of blue decorations. This situation did not allow for performing FF-XANES investigations at Co K-edge as previously done. The absorption before the Co K-edge is too strong because of the significant iron absorption. A reduction of the sample thickness would decrease the Fe absorption but would also decrease the Co absorption, making it unmeasurable. Consequently, FF-XANES investigations have been possible only at the Fe K-edge.

## 4. Conclusion

FF-XANES analysis is a very powerful technique to study complex structure and provide pertinent chemical information. It combines spatial and energy resolution with large FOVs and fast acquisition in a virtually limitless variety of samples. The spatial resolution can be adapted to the problematic from a few hundred to a few tens of nanometer following the geometry used (defocalized beam or transmission X-ray microscope). Software packages, such as TXM-Wizard or PyMca, provide user-friendly tools to successfully plan and collect the series of radiographies, to build from these images the 2D XANES map (advanced averaging, image alignment, filtering), and to process these big data in order to extract chemical information such as rate, valence state, and speciation. These tools are rather easy to use and allow obtaining pertinent information in the form of easily exploitable maps.

This technique combines XANES analysis (selectivity) and mapping of large areas at high revolution advantages. For complex systems consisting of many elements, the possibility to focus on specific key element is fundamental, while for heterogeneous system, the possibility to investigate a large area with a high spatial resolution is essential. FF-XANES analysis is thus ideally suited for studying complex and heterogeneous materials such as materials involved in the conception of ancient objects. In particular, the relationships between a specific physical property and the involved elements are quickly determined. For instance, in the second example presented in previous paragraphs, the distribution and the speciation of transition elements to the color are linked. In the first example of reverse engineering, iron is the key element to identify the firing process and the selectivity of technique allows focusing on the Fe-based phases without being disturbed by the other phases. This technique begins to be used with success on other cultural heritage material types such as pigment in paintings of Henri Matisse [21].

This analytical technique is based on measurements in transmission mode, which implies a specific preparation of samples and the limitations of the collecting XANES spectra as illustrated in the first example.

Of course, this interesting technique is not reserved to cultural heritage materials, and several other examples of study can be found in the literature concerning different material types [22–26]. Full-field-based techniques are still in development and become more and more available on synchrotron beamlines such as, for instance on PUMA, a beamline at SOLEIL (French synchrotron, Saclay) dedicated to the study of cultural heritage materials.

## Acknowledgements

## Author details

Philippe Sciau[1]* and Tian Wang[2]*

1 CEMES-CNRS, Toulouse University, Toulouse, France

2 School of Materials Science and Engineering, Shaanxi University of Science and Technology, Xi'an, PR China

*Address all correspondence to: philippe.sciau@cemes.fr and wangtian@sust.edu.cn

**IntechOpen**

## References

[1] Bertrand L, Cotte M, Stampanoni M, Thoury M, Marone F, Schöder S. Development and trends in synchrotron studies of ancient and historical materials. Development and Trends in Synchrotron Studies of Ancient and Historical Materials. 2012;**519**:51-96. DOI: 10.1016/j.physrep.2012.03.003

[2] Cotte M, Pouyet E, Salome M, Rivard C, De Nolf W, Castillo-Michel H, et al. The ID21 X-ray and infrared microscopy beamline at the ESRF: Status and recent applications to artistic materials. Journal of Analytical Atomic Spectrometry. 2017;**32**:477-493. DOI: 10.1039/c6ja00356g

[3] Sciau P, Goudeau P. Ceramics in art and archaeology: A review of the materials science aspects. European Physical Journal B. 2015;**88**:132. DOI: 10.1140/epjb/e2015-60253-8

[4] Cotte M, Genty-Vincent A, Janssens K, Susini J. Applications of synchrotron X-ray nano-probes in the field of cultural heritage. Comptes Rendus Physique. 2018;**19**:578-588. DOI: 10.1016/j.crhy.2018.07.002

[5] Dejoie C, Tamura N, Kunz M, Goudeau P, Sciau P. Complementary use of monochromatic and white-beam X-ray micro-diffraction for the investigation of ancient materials. Journal of Applied Crystallography. 2015;**48**:1522-1533. DOI: 10.1107/S1600576715014983

[6] Monico L, Janssens K, Alfeld M, Cotte M, Vanmeert F, Ryan CG, et al. Full spectral XANES imaging using the Maia detector array as a new tool for the study of the alteration process of chrome yellow pigments in paintings by Vincent van Gogh. Journal of Analytical Atomic Spectrometry. 2015;**30**:613-626. DOI: 10.1039/C4JA00419A

[7] Meirer F, Cabana J, Liu Y, Mehta A, Andrews JC, Pianetta P. Three-dimensional imaging of chemical phase transformations at the nanoscale with full-field transmission X-ray microscopy. Journal of Synchrotron Radiation. 2011;**18**:773-781. DOI: 10.1107/S0909049511019364

[8] Chu YS, Yi JM, De Carlo F, Shen Q, Lee W-K, Wu HJ, et al. Hard-X-ray microscopy with Fresnel zone plates reaches 40nm Rayleigh resolution. Applied Physics Letters. 2008;**92**:103119. DOI: 10.1063/1.2857476

[9] Liu Y, Andrews JC, Wang J, Meirer F, Zhu P, Wu Z, et al. Phase retrieval using polychromatic illumination for transmission X-ray microscopy. Optics Express. 2011;**19**:540-545. DOI: 10.1364/OE.19.000540

[10] Solé VA, Papillon E, Cotte M, Walter P, Susini J. A multiplatform code for the analysis of energy-dispersive X-ray fluorescence spectra. Spectrochimica Acta Part B: Atomic Spectroscopy. 2007;**62**:63-68. DOI: 10.1016/j.sab.2006.12.002

[11] Liu Y, Meirer F, Williams PA, Wang J, Andrews JC, Pianetta P. TXM-wizard: A program for advanced data collection and evaluation in full-field transmission X-ray microscopy. Journal of Synchrotron Radiation. 2012;**19**:281-287. DOI: 10.1107/S0909049511049144

[12] Sciau P, Leon Y, Goudeau P, Fakra SC, Webb S, Mehta A. Reverse engineering the ancient ceramic technology based on X-ray fluorescence spectromicroscopy. Journal of Analytical Atomic Spectrometry. 2011;**26**:969-976. DOI: 10.1039/c0ja00212g

[13] Meirer F, Liu Y, Pouyet E, Fayard B, Cotte M, Sanchez C, et al. Full-field XANES analysis of Roman ceramics

to estimate firing conditions—A novel probe to study hierarchical heterogeneous materials. Journal of Analytical Atomic Spectrometry. 2013;**28**:1870-1883. DOI: 10.1039/c3ja50226k

[14] Wang T. A multi-scale study of ancient ceramics using a series of analytical techniques [PhD thesis]. Toulouse University; 2016

[15] Paleo P, Pouyet E, Kieffer J. Image stack alignment in full-field X-ray absorption spectroscopy using SIFT_PyOCL. Journal of Synchrotron Radiation. 2014;**21**:456-461. DOI: 10.1107/S160057751400023X

[16] Cianchetta I, Trentelman K, Maish J, Saunders D, Foran B, Walton M, et al. Evidence for an unorthodox firing sequence employed by the Berlin painter: Deciphering ancient ceramic firing conditions through high-resolution material characterization and replication. Journal of Analytical Atomic Spectrometry. 2015;**30**:666-676. DOI: 10.1039/c4ja00376d

[17] Wen R, Wang CS, Mao ZW, Huang YY, Pollard AM. The chemical composition of blue pigment on Chinese blue-and-white porcelain of the Yuan and Ming dynasties (AD 1271-1644). Archaeometry. 2007;**49**:101-115. DOI: 10.1111/j.1475-4754.2007.00290.x

[18] Wang T, Zhu TQ, Feng ZY, Fayard B, Pouyet E, Cotte M, et al. Synchrotron radiation-based multi-analytical approach for studying underglaze color: The microstructure of Chinese Qinghua blue decors (Ming dynasty). Analytica Chimica Acta. 2016;**928**:20-31. DOI: 10.1016/j.aca.2016.04.053

[19] Calvin S. XAFS for Everyone. Boca Raton: CRC Press; 2013

[20] Qu Y, Xu J, Xi X, Huang C, Yang J. Microstructure characteristics of blue-and-white porcelain from the folk kiln of Ming and Qing dynasties. Ceramics International. 2014;**40**:8783-8790. DOI: 10.1016/j.ceramint.2014.01.100

[21] Pouyet E, Cotte M, Fayard B, Salomé M, Meirer F, Mehta A, et al. 2D X-ray and FTIR micro-analysis of the degradation of cadmium yellow pigment in paintings of Henri Matisse. Applied Physics A: Materials Science & Processing. 2015;**121**:967-980. DOI: 10.1007/s00339-015-9239-4

[22] Harris WM, Nelson GJ, Izzo JR, Grew KN, Chiu WKS, Chu YS, et al. Full Field Imaging of Nickel Oxidation States in Solid Oxide Fuel Cell Anode Materials by XANES Nanotomography. New York: Amer Soc Mechanical Engineers; 2012

[23] Boesenberg U, Meirer F, Liu Y, Shukla AK, Dell'Anna R, Tyliszczak T, et al. Mesoscale phase distribution in single particles of $LiFePO_4$ following lithium deintercalation. Chemistry of Materials. 2013;**25**:1664-1672. DOI: 10.1021/cm400106k

[24] Yang F, Liu Y, Martha SK, Wu Z, Andrews JC, Ice GE, et al. Nanoscale morphological and chemical changes of high voltage lithium manganese rich NMC composite cathodes with cycling. Nano Letters. 2014;**14**:4334-4341. DOI: 10.1021/nl502090z

[25] Hesse B, Salome M, Castillo-Michel H, Cotte M, Fayard B, Sahle CJ, et al. Full-field calcium K-edge X-ray absorption near-edge structure spectroscopy on cortical bone at the micron-scale: Polarization effects reveal mineral orientation. Analytical Chemistry. 2016;**88**:3826-3835. DOI: 10.1021/acs.analchem.5b04898

[26] Sorbadere F, Laurenz V, Frost DJ, Wenz M, Rosenthal A, McCammon C, et al. The behaviour of ferric iron during partial melting of peridotite. Geochimica et Cosmochimica Acta. 2018;**239**:235-254. DOI: 10.1016/j.gca.2018.07.019